

# Numerical simulation of the influence of major meteorological elements on the concentration of air pollutants during rainfall over Sichuan Basin of China



Wei Long<sup>a</sup>, Yunjun Zhou<sup>a,b,\*</sup>, Ping Liu<sup>c</sup>

<sup>a</sup> College of Atmospheric Sciences, Chengdu University of Information & Technology, Chengdu, 610225, China

<sup>b</sup> Collaborative Innovation Center on Forecast and Evaluation of Meteorological Disasters, Nanjing University of Information Science and Technology, Nanjing, 210044, China

<sup>c</sup> Weather Modification Office of Sichuan Province, Chengdu, 610225, China

## ARTICLE INFO

### Keywords:

WRF-Chem model  
Air pollutants  
Rainfall  
Scavenging  
Circulations

## ABSTRACT

To study the wet removal effect of rainfall on the air pollutants in Sichuan Basin, the WRF-Chem model is adopted to simulate the changes of air pollutant concentrations before and after a rainfall episode. The results show that continuous rainfall with small-magnitude rainfall ( $0.3\text{--}0.5 \text{ mm h}^{-1}$ ) has an obvious effect in reducing the concentrations of  $\text{PM}_{2.5}$ ,  $\text{PM}_{10}$ ,  $\text{SO}_2$  and  $\text{NO}_2$  except for  $\text{O}_3$ . There is an upper limit of the impact of continuous rainfall on air pollutants. The reduction of concentrations of particulate pollutants at the level of 300–2500 m is due to its participation in the nucleation process. When rainfall occurs and vertical diffusion is not restricted, the concentration of pollutants on the ground are reduced more quickly by being transported to high altitude. In urban areas with near-surface inversion, there is an anti-correlation between concentrations and wind speed. The correlation coefficients for the concentrations of  $\text{PM}_{2.5}$ ,  $\text{PM}_{10}$ ,  $\text{SO}_2$  and  $\text{NO}_2$  with the wind speed are  $-0.85$ ,  $-0.86$ ,  $-0.77$  and  $-0.82$ , respectively. In suburban stations with the small initial concentrations, the decrease of concentrations is mainly due to the increase of rainfall intensity, but has little relationship with the height of PBL and the wind speed. The small gradient of sea level pressure (less than 1 hPa) and the near-surface inversion in the Chengdu Plain are conducive to the accumulation of air pollutants.

## 1. Introduction

In recent years, air pollution in China has become increasingly serious. Air pollutants such as particulate matter, ozone, nitrogen oxides and sulphides in the atmosphere are threatening human health, and thus it has become a focus of our society. When pollution sources are relatively stable, meteorological fields such as temperature, pressure, humidity, wind direction, wind speed, precipitation and atmospheric stability are the main elements affecting the concentrations of air pollutants. Among them, the effects of precipitation and wind on aerosols are important for the atmospheric self - cleaning (Tie et al., 2015).

Many scholars have discussed the wet removal of aerosols with different scales through observations. They have found that the precipitation has a significant removal effect on aerosol particles with diameters less than  $0.1 \mu\text{m}$  and larger than  $2 \mu\text{m}$ , while the effect on aerosol particles with the diameter ranging from  $0.2$  to  $2 \mu\text{m}$  is poor,

that is, there is a "Greenfield gap" (Greenfield, 1956) in the removal of aerosol particles by precipitation. The above studies have shown that there is a positive correlation between the rainfall intensity and wet removal (Chate et al., 2005; Kang et al., 2009; Zhao et al., 2015; Dong et al., 2016). Besides, the wet removal effect on different air pollutants has also been investigated. Li and Wang (2007) and Zhou et al. (2013) studied the ability of precipitation with different intensities in removing  $\text{PM}_{10}$ ,  $\text{SO}_2$  and  $\text{NO}_2$ . The results indicated that precipitation has the best removal effect on  $\text{PM}_{10}$ , followed by  $\text{SO}_2$  and  $\text{NO}_2$ , and the wet removal ability of heavy rain (12.1–24 mm/day) to  $\text{SO}_2$  and  $\text{PM}_{10}$  is the greatest, followed by light rain (0.3–6 mm/day) and moderate rain (6.1–12 mm/day). Similar effects can also be found on  $\text{NO}_2$ . Zou et al. (2017) found that due to different mechanisms, the removal efficiency of rainfall to particulate pollutants is higher than that to gaseous pollutants which depends on the water solubility. Moreover, the removal efficiency on air pollutants is positively correlated with the relative humidity. Zhou et al. (2015) found that the higher the concentrations of particulate

Peer review under responsibility of Turkish National Committee for Air Pollution Research and Control.

\* Corresponding author. College of Atmospheric Science, Chengdu University of Information & Technology, 24 Xuefu Road, Chengdu, 610225, China.

E-mail address: [zhouyj@cuit.edu.cn](mailto:zhouyj@cuit.edu.cn) (Y. Zhou).

matters before the rainfall, the higher the removal efficiency. In different seasons, the initial thresholds of concentrations for positive removal effect are different (Geng et al., 2019). When the initial concentrations of pollutants are very low, the rainfall might even increase the concentrations (Liu et al., 2016). The variation in PM<sub>2.5</sub> concentrations is not only related to the initial concentrations, but also to the rainfall intensity and rainfall duration (Yu et al., 2018). The above-mentioned researchers used external field observations and experimental methods to study the atmospheric environmental problems. Limited data restricted the study of regional air pollution processes and the spatial distribution. Therefore, it is necessary to use numerical models besides improving the monitoring network for observational research. The chemical transport model used in this study is the Weather Research and Forecasting model coupled with Chemistry (WRF-Chem), which is an on-line model that simulates the transport, mixing and chemical transformation of trace gases and aerosols simultaneously with meteorological fields (Grell et al., 2005). In recent years, the WRF-Chem has been widely used in regional air pollution simulation research in North America, Europe and Asia (Tie et al., 2009; Misenis et al., 2010; Tuccella et al., 2012; He et al., 2016). In China, studies on air pollution by using WRF-Chem are mostly carried out in North China (Pang et al., 2013; Zhang et al., 2015; Wang et al., 2016), but few in Sichuan Basin.

In recent decades, air pollution in Sichuan Basin has become increasingly severe due to its unique meteorological and topographic conditions, the formation, transport, and distribution of pollutants (Zhao et al., 2019). Limited by air pollution monitoring data, previous studies mostly focused on the variation characteristics of certain pollutants with time and the synoptic pattern during severe air pollution in Sichuan Basin (Zeng et al., 2017; Liao et al., 2017; Long et al., 2019; Jiang et al., 2019; Ouyang et al., 2019), but little research has been done about the wet removal of air pollutants. Yang et al. (2018) once studied the effects of rainfall in June and July on the concentrations of particulates and gaseous pollutants in Chengdu, but the spatial resolution was too coarse to accurately reflect the variations of atmospheric pollutant concentrations within the rainfall process as the precipitation data at Wenjiang station was taken as the average for Chengdu. Besides, the air pollution is not serious in summer. Therefore, it is necessary to use numerical models to further study the effects of rainfall on removing atmospheric pollutants when air pollution frequently occurs. Based on the simulation of an autumn rainfall process in Sichuan Basin with the WRF-Chem, the temporal and spatial distributions as well as the evolution of PM<sub>2.5</sub>, PM<sub>10</sub>, NO<sub>2</sub>, SO<sub>2</sub> and O<sub>3</sub> concentrations before and after the rainfall are analyzed, the weather pattern when air pollutants accumulate as well as the wet removal effect of rainfall on different air pollutants are also discussed. This paper aims to provide a reference and technical support for air pollution control, the early warning of air quality, and the selection of parameterization schemes in numerical simulation for air pollution episodes in Sichuan Basin.

## 2. Methods

### 2.1. Data and model

The chemical transport model used in this study is the WRF-Chem, version 3.9.1. The simulation period contains 48 h from 2000 BST (Beijing standard time, the same below) on October 16 to 2000 BST on October 18, 2018, with the first day as a spin-up. The Final Operational Global Analysis (FNL) of National Centers for Environmental Prediction (NCEP) data shows that a synoptic pattern of two-trough and one-ridge type appeared on the 500 hPa circulation at 2000 BST on October 17 in the middle and high latitudes of Eurasia (Fig. 1). The two troughs were located over the Ural Mountains and Northeast China, and the ridge was located over the north of Mongolia. Meanwhile, the northwest airflow at 500 hPa dominated Sichuan Basin. The low-altitude low

southwesterly wind was slow, making it difficult to transport the water vapor from the Bay of Bengal to the basin. Above-mentioned circulation patterns are commonly seen when air pollution occurs in Chengdu (Zeng et al., 2016). The characteristics of the surface weather system show that the sea level pressure variation in the Chengdu Plain was very small, and there was an inversion layer at low levels over this region (Fig. 2). Under this weather pattern, air pollutants tended to accumulate in the basin, thus leading to slight air pollution in Chengdu, Meishan, Zigong and other places on the same day. Since 0200 BST on October 18, the weather system gradually moved eastward, and Sichuan Basin was mainly controlled by the southwesterly airflow. In addition, under the influence of the water vapor from the South China Sea brought by southeasterly wind and the southwesterly warm-wet airflow, rainfall formed in many areas of Sichuan Basin.

A single-domain simulation is used in the study area (Fig. 3), with horizontal grids of 471 × 426, and the center point is located in 103.5°E, 30.5°N. The horizontal resolution is 3 km, with 31 layers in the vertical direction. The 6-h NCEP FNL data with longitude-latitude resolution of 1° × 1° provide the initial and lateral boundary meteorological conditions for WRF-Chem. The most recent anthropogenic emission inventories for 2016 developed by Tsinghua University are also used in this study (<http://www.meicmodel.org>). Emissions with the finest resolution of 0.25° × 0.25° are adopted for the simulations here. A dynamic, technology-based methodology for all the anthropogenic emissions is utilized in the Multi-resolution Emission Inventory for China (MEIC) inventories (Zhang et al., 2009; Li et al., 2014; Zheng et al., 2014; Liu et al., 2015). Programs referring to WRF-Chem emissions document ([https://ruc.noaa.gov/wrf/wrf-chem/Emission\\_guide.pdf](https://ruc.noaa.gov/wrf/wrf-chem/Emission_guide.pdf)) are used to construct the emission dataset for the domain and desired chemistry option from inventories. A built-in program in WRF-Chem is used to create the initial and boundary chemical conditions. The model configurations used in this study are shown in Table 1, and the particle dry-diameter ranges for 8-bin MOSAIC are shown in Table 2. As can be seen, no cumulus parameterization scheme is adopted. For WRF model, the cumulus parameterization scheme is suitable for coarse grids at the resolution of larger than 10 km. In areas with strong convection, cumulus parameters can also be considered at high resolutions, but it is generally not used when the resolution is less than 5 km. The model divides the scavenging by rainfall into two processes: first, in-cloud, or nucleation scavenging (rainout), which is the local uptake of soluble gases and aerosols by the formation of initial cloud droplets and their conversion to precipitation; second, below-cloud, or impaction scavenging (washout), which is the collection of soluble species from the interstitial air by falling hydrometeors. The simulation turns on the feedback effects of wet scavenging, cloud chemistry and aerosol-radiation, as well as the urban surface scheme to better reflect the changes in local circulation and the types of urban underlying surfaces. Note that the WRF-Chem uses a terrain following coordinate system, so the heights mentioned in the article are the heights above ground level.

### 2.2. Model evaluation data set and protocols

Chengdu is selected as the assessment object. The hourly observation data of air pollutant concentrations are obtained from 8 air quality monitoring stations in Chengdu, including PM<sub>2.5</sub>, PM<sub>10</sub>, SO<sub>2</sub>, NO<sub>2</sub> and O<sub>3</sub>. The locations of the stations are marked in Fig. 3, among which, Lingyansi (LYS) is located in the northwest edge of the Chengdu Plain, with relatively less pollution discharge and better air quality, while Longquan is far away from the city center. The other six stations are located in the area within the Third Ring Road of Chengdu, representing the stations in the central urban area of Chengdu. The surface weather observations are derived from 156 weather stations in Sichuan Province, including variables such as temperature, air pressure, relative humidity, wind speed, wind direction and precipitation.

The meteorological evaluation is performed in terms of domain-

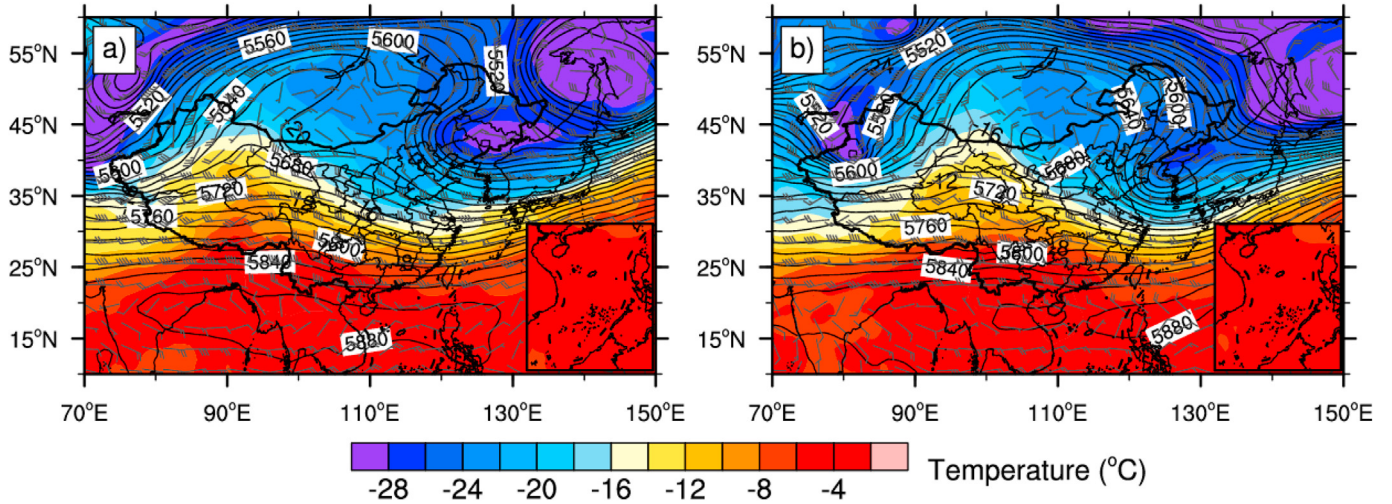


Fig. 1. Circulation pattern at 500 hPa: a) 2000 BST on 17 October, b) 0200 BST on 18 October.

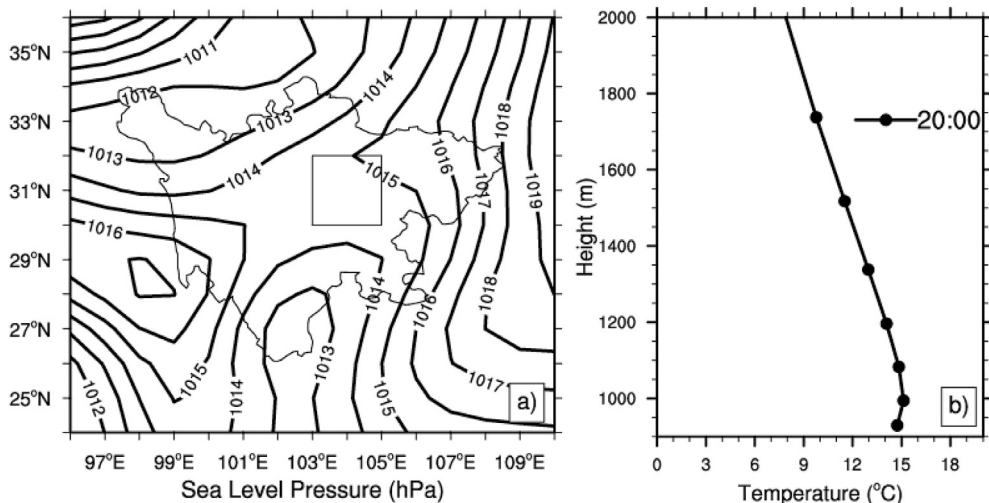


Fig. 2. a) Distribution of sea level pressure, b) Profile of average temperature in the box area at 2000 BST on 17 October (Pollutants accumulated in the box area).

wide overall statistics. The following basic statistical indicators are used for evaluation: the mean bias (*MB*), the normalized mean bias (*NMB*), the normalized mean error (*NME*), the hit rate (*HR*), the mean fractional bias (*MFB*), and the mean fractional error (*MFE*). The *HR* represents the percentage of data pairs whose difference between the observed and simulated values involved in the statistics is less than the specified standard. The standards are as follows (Zhang et al., 2012). The difference is less than 2 K in temperature; less than  $1\text{m}\cdot\text{s}^{-1}$  in wind speed; and less than  $30^\circ$  in wind direction. In this paper, the relative humidity standard is set to less than 20%. Relevant definitions of each statistical index are as follows.

$$\text{MB} = \frac{1}{N} \sum_{i=1}^N (C_m - C_0)$$

$$\text{NMB} = \frac{\sum_{i=1}^N (C_m - C_0)}{\sum_{i=1}^N C_0} \times 100\%$$

$$\text{NME} = \frac{\sum_{i=1}^N |C_m - C_0|}{\sum_{i=1}^N C_0} \times 100\%$$

$$\text{MFB} = \frac{1}{N} \sum_{i=1}^N \frac{(C_m - C_0)}{(C_0 + C_m/2)} \times 100\%$$

$$\text{MFE} = \frac{1}{N} \sum_{i=1}^N \frac{|C_m - C_0|}{(C_0 + C_m/2)} \times 100\%$$

where *N* is the number of samples involved in the statistics,  $C_m$  and  $C_0$  are the simulated and observed values, respectively.

The chemical evaluation is performed by using the *MFB* and *MFE*. Boylan and Russell (2006) proposed that a satisfactory performance is indicated by an *MFB* within  $\pm 60\%$ , and an *MFE* within 75%; a superior performance is indicated by an *MFB* within  $\pm 30\%$ , and an *MFE* within 50%.

### 3. Model performance evaluation

#### 3.1. Meteorological evaluation

Table 3 shows the performance statistics for meteorological field simulations. The predicted near surface temperature (*T<sub>2</sub>*) is higher than the observation all the time with the *MB* of  $1.68^\circ\text{C}$  and the *HR* of 48.28%. The predicted relative humidity at 2 m (*RH<sub>2</sub>*) is lower than the observation with the *MB* of  $-15.56\%$  and the *HR* of 65.52%. As the predicted *T<sub>2</sub>* is higher than the observation, the predicted *RH<sub>2</sub>* is somewhat lower. The bias of *T<sub>2</sub>* and *RH<sub>2</sub>* may be influenced by the planetary boundary layer (PBL) scheme, which is used to calculate the turbulent flux of physical quantities such as the heat and momentum in

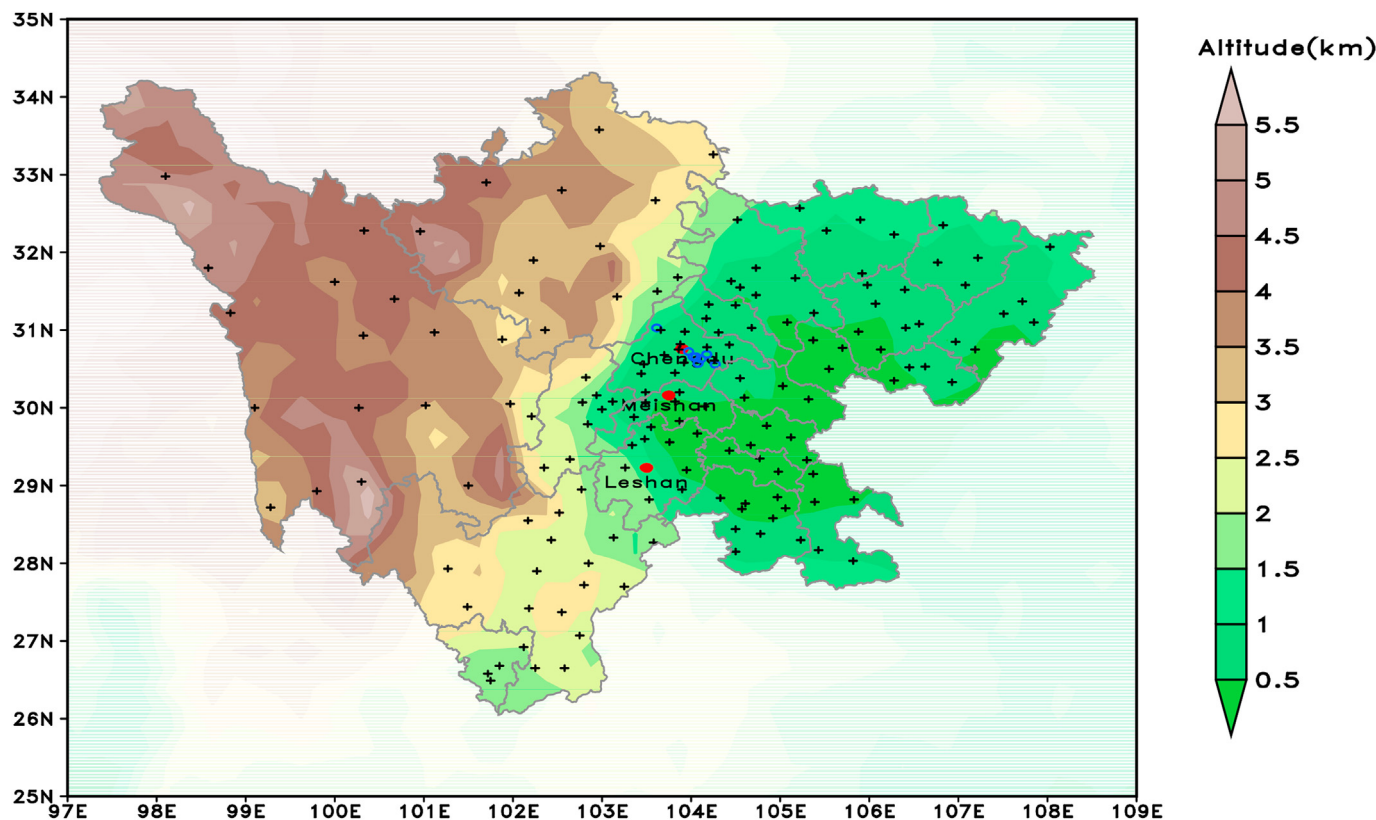


**Fig. 3.** Schematic diagram of location of both meteorological stations (black markers) and air-quality stations (blue markers). (For interpretation of the references to colour in this figure legend, the reader is referred to the Web version of this article.)

**Table 1**  
Model configurations<sup>a</sup>.

Process	Options
Microphysics	Lin (Purdue) microphysics [Lin et al., 1983]
Long-wave radiation	RRTMG (Rapid Radiative Transfer Model for General circulation models) [Iacono et al., 2008]
Short-wave radiation	RRTMG [Iacono et al., 2008]
Land surface model (LSM)	Noah LSM [Chen and Dudhia 2001]
Planetary boundary layer (PBL)	MYNN (Mellor-Yamada-Nakanishi-Niino) Level 2.5 PBL [Nakanishi and Niino 2006]
Cumulus parameterization	\
Gas-phase chemistry	CBM-Z (Carbon Bond Mechanism-Z) [Zaveri and Peters 1999]
Aerosol module	8-bin MOSAIC (Model for Simulating Aerosol Interactions and Chemistry) [Zaveri et al., 2008]
Photolysis	Fast-J [Wild et al., 2000]

<sup>a</sup> Please refer to the model user's guide for a complete description of these options ([https://ruc.noaa.gov/wrf/wrf-chem/Users\\_guide.pdf](https://ruc.noaa.gov/wrf/wrf-chem/Users_guide.pdf)).

**Table 2**  
Particle dry-diameter range for the eight size bins employed by MOSAIC.

Size bin	upper bound (μm)	upper bound (μm)
1	0.0390625	0.78125
2	0.078125	0.15625
3	0.15625	0.3125
4	0.3125	0.625
5	0.625	1.25
6	1.25	2.5
7	2.5	5.0
8	5.0	10.0

the boundary layer (Holt et al., 1988). Different boundary layer schemes result in different strengths of vertical mixing and entrainments of air from above the PBL, which may lead to large differences in temperature and humidity in the boundary layer (Hu et al., 2010). The model reproduces the T2 and RH2 with a correlation of 0.52 and 0.60 respectively, and the NMBs of both T2 and RH2 are less than 20%, so

**Table 3**  
Performance Statistics for meteorological elements.

	T2 (°C)	RH2 (%)	WS10 (m s <sup>-1</sup> )	WD10 (°)	Rain (mm)
MB	1.68	-15.56	0.15	12.61	-0.01
HR (%)	48.28	65.52	93.10	44.83	\
NMB (%)	13.54	-19.40%	13.39	13.81	-4.80
NME (%)	13.62	19.40%	26.82	48.62	47.75
R	0.523 <sup>a</sup>	0.600 <sup>a</sup>	0.661 <sup>a</sup>	0.432 <sup>a</sup>	0.513 <sup>a</sup>
P value	0.004	0.001	0.000	0.008	0.009

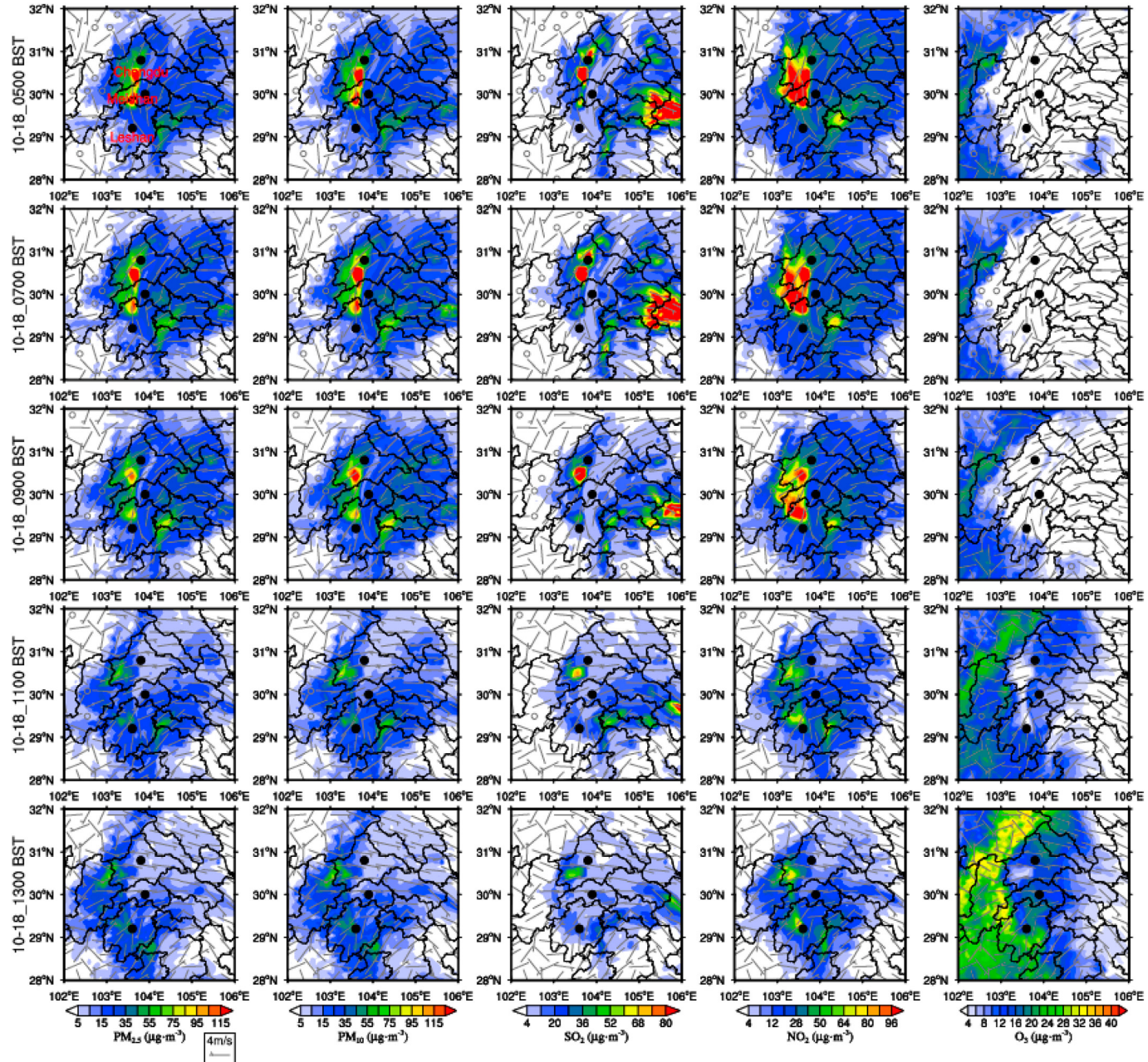
<sup>a</sup> Statistically significant at 99% confident level.

the model performance of near surface temperature and relative humidity could be considered satisfactory. The MBs of 10 m wind speed (WS10) and wind direction (WD10) are 0.15 m s<sup>-1</sup> and 12.61°, respectively. The HR reaches 93.10% for WS10, and 44.83% for WD10. The correlations are 0.66 for WS10 and 0.43 for WD10. Due to the particularity of wind direction statistics, the MB is high while the HR is low. For example, there is only a slight difference of 20° between the

**Table 4**

Performance Statistics for major air pollutants.

	$\text{PM}_{2.5} (\mu\text{g}\cdot\text{m}^{-3})$	$\text{PM}_{10} (\mu\text{g}\cdot\text{m}^{-3})$	$\text{SO}_2 (\mu\text{g}\cdot\text{m}^{-3})$	$\text{NO}_2 (\mu\text{g}\cdot\text{m}^{-3})$	$\text{CO} (\mu\text{g}\cdot\text{m}^{-3})$	$\text{O}_3 (\mu\text{g}\cdot\text{m}^{-3})$
MB	-14.72	-21.68	20.41	-3.71	-0.028	-23.34
NMB (%)	-34.62	-39.35	301.47	-10.78	-4.37	-75.59
MFB (%)	-26.96	-31.22	76.64	-12.62	-12.21	-71.27
MFE (%)	30.68	34.75	78.81	28.13	39.59	71.27
R	0.680 <sup>a</sup>	0.676 <sup>a</sup>	0.610 <sup>a</sup>	0.597 <sup>a</sup>	0.390	0.514 <sup>b</sup>
P value	0.000	0.000	0.002	0.003	0.066	0.012

<sup>a</sup> Statistically significant at 99% confident level.<sup>b</sup> Statistically significant at 95% confident level.**Fig. 4.** The horizontal distributions of  $\text{PM}_{2.5}$ ,  $\text{PM}_{10}$ ,  $\text{SO}_2$ ,  $\text{NO}_2$  and  $\text{O}_3$  in Sichuan Province at 0500, 0700, 0900, 1100 and 1300 BST on 18 October, 2018 (Units:  $\mu\text{g}\cdot\text{m}^{-3}$ ).

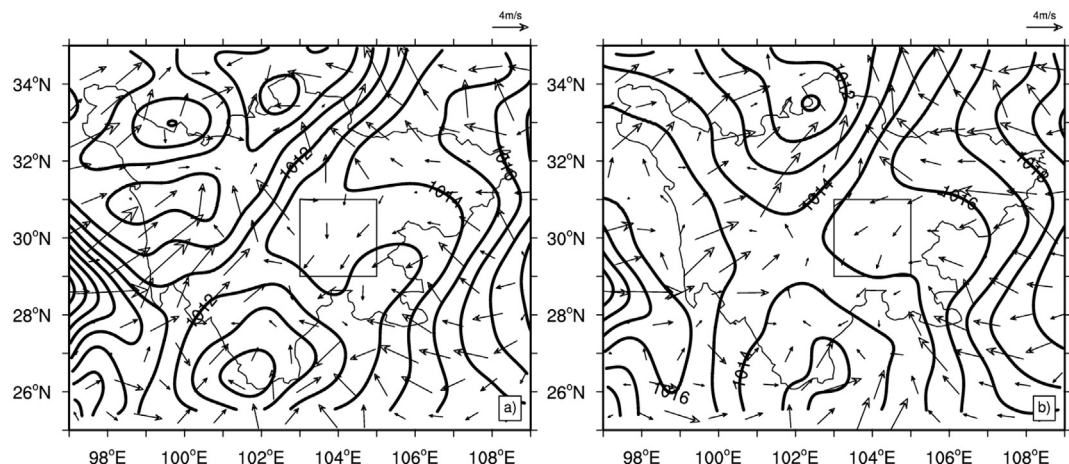


**Fig. 5.** Distribution of sea level pressure at 2000 BST (a) on 17 October and 0800 BST (b) on 18 October, 2018 (Pollutants accumulated in the box area).

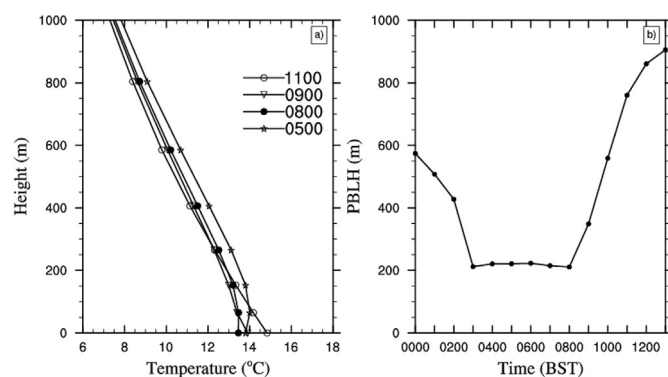


**Fig. 6.** Vertical profiles of mean air temperature (a) and mean height of PBLH (b) in the box area.

wind direction of  $350^\circ$  and  $10^\circ$ , but the calculated difference is  $340^\circ$ . Therefore, we believe that the WRF-Chem model can well simulate WS10 and WM10. The model reproduces the rain with a correlation of 0.51 and a small bias of  $-0.11$ , due to underestimation of rainfall in the early stage.

### 3.2. Chemical evaluation

The simulation performances for  $\text{PM}_{2.5}$ ,  $\text{PM}_{10}$ ,  $\text{NO}_2$  and  $\text{CO}$  concentrations almost all reach the standard of superior performance, with  $MFBs$  of  $-26.96\%$ ,  $-31.22\%$ ,  $-12.62\%$  and  $-12.21\%$ , respectively (Table 4). The simulation underestimates most air pollutant concentrations by  $34.62\%$ ,  $39.35\%$ ,  $10.78\%$  and  $4.37\%$  for  $\text{PM}_{2.5}$ ,  $\text{PM}_{10}$ ,  $\text{NO}_2$  and  $\text{CO}$  concentrations, respectively, and even  $75.59\%$  for  $\text{O}_3$ . However, the over-prediction bias of  $\text{SO}_2$  exceeds  $300\%$ . One possible reason is that the emission inventories may be subjected to the uncertainty in allocating those emissions into grids with fine resolutions (Wang et al., 2016). Another uncertainty appears in the difference between the base year (2016) and simulation period (October 2018) for the emissions. The total anthropogenic emissions of  $\text{SO}_2$  may have been overestimated due to the 13th Five-Year Plan (2016–2020) for energy conservation and emission reduction. Large biases appear in the simulation of  $\text{SO}_2$  and  $\text{O}_3$  concentrations, but the trends between the simulations and observations are relatively consistent. The Pearson's correlation coefficients of  $\text{SO}_2$  and  $\text{O}_3$  are 0.61 and 0.51 and pass the significance tests at 99% and 95% confidence levels, respectively.

There are different degrees of biases in the initial concentrations of  $\text{PM}_{2.5}$ ,  $\text{PM}_{10}$  and  $\text{NO}_2$  output from the model, but their decreasing trends with the variations in meteorological fields are closer to the

observations (Fig. 9a – e). For  $\text{O}_3$ , a fluctuation from 1200 to 2200 BST on October 17 is not reproduced, presenting a large negative bias, possibly due to the coarse resolution of emission sources for the model, or the incapability of the model in reflecting accidental emission events. The  $MFB$  ( $MFE$ ) of  $\text{PM}_{2.5}$ ,  $\text{PM}_{10}$ ,  $\text{NO}_2$  and  $\text{CO}$  concentrations ranges from  $-12.21\%$  to  $-31.22\%$  ( $28.13\%$ – $39.59\%$ ). According to the performance standards of  $MFBs$  within  $\pm 60\%$  and  $MFEs$  within  $\pm 75\%$  proposed by Boylan and Russell (2006), the simulation performances of  $\text{PM}_{2.5}$ ,  $\text{PM}_{10}$ ,  $\text{NO}_2$  and  $\text{CO}$  by WRF-Chem are satisfactory. Significant correlations exist between the simulations and observations of  $\text{SO}_2$  and  $\text{O}_3$ . The  $MFE$  of  $\text{SO}_2$  is  $78.81\%$ , slightly higher than the performance standard of  $75\%$ , and the  $MFE$  of  $\text{O}_3$  is  $71.27\%$ , still within the standard range.

In the evaluation at Chengdu, the WRF-Chem performs well in simulating the average temperature, humidity, wind direction, wind speed and precipitation, and the variation trends for concentrations of major pollutants can also be reproduced. As the topography and circulation patterns across the Chengdu Plain are generally consistent (Figs. 1–3), it is of practical significance to apply the model results to the analysis for other areas of the Chengdu Plain. In addition, the model includes in-cloud scavenging, and the process of nucleation is easier to remove soluble and chemically active trace gases, while the solubility of  $\text{CO}$  is very poor, so it is not discussed in this paper.

## 4. Results and discussion

### 4.1. Distribution of air pollutants in Sichuan Basin

The spatial distribution of major air pollutants indicates (Fig. 4) that there was an air pollutant accumulation area on the ground in the Chengdu Plain at 0500 BST on October 18, with the pollutants mainly concentrated in the southwestern Chengdu and northern Leshan. The maximum  $\text{PM}_{2.5}$  and  $\text{PM}_{10}$  concentrations in the region exceeded  $115 \mu\text{g m}^{-3}$  while the  $\text{O}_3$  concentrations was very low. By 1300 BST on October 18, the  $\text{PM}_{2.5}$  and  $\text{PM}_{10}$  concentrations in this region had decreased to  $5$ – $55 \mu\text{g m}^{-3}$  and  $5$ – $65 \mu\text{g m}^{-3}$ , respectively. The  $\text{SO}_2$  and  $\text{NO}_2$  concentrations decreased by about  $40 \mu\text{g m}^{-3}$  during this period. The  $\text{O}_3$  concentrations increased in most areas, but the values were still small. The source of  $\text{O}_3$  is not further analyzed in this paper.

By analyzing the mean values of some meteorological factors in the polluted areas, the causes for the concentration variations of 5 kinds of air pollutants from 0500 BST to 1300 BST on October 18, 2018 are studied. At 0800 on October 18, no obvious active high-level trough appeared over the polluted area, and the atmosphere over Sichuan was controlled by a westerly airflow. The surface weather pattern shows that the gradient of the sea level pressure and the wind speed in the

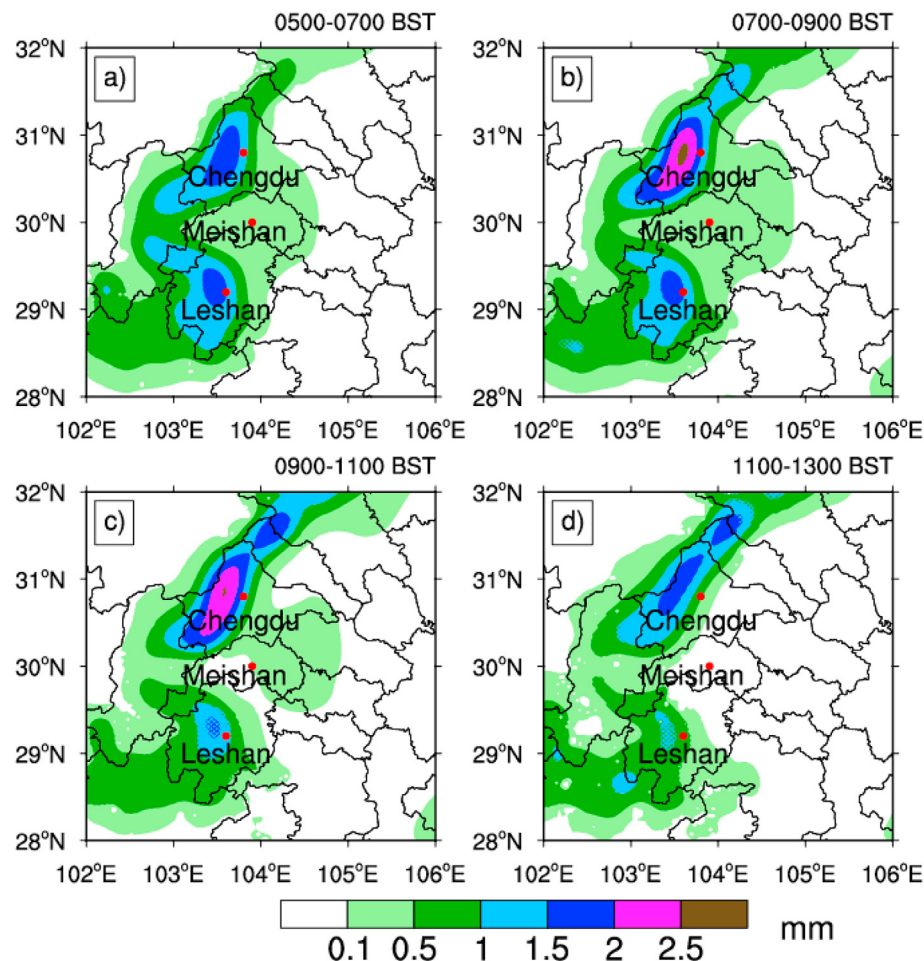


**Fig. 7.** Two-hours accumulation precipitation from 0500 to 0700 BST (a), 0700 to 0900 BST (b), 0900 to 1100 BST (c) and 1100 to 1300 BST (d) on 18 October, 2018.

polluted area were small, the average wind speed was less than  $1.3 \text{ m s}^{-1}$  before 0900 BST, thereby the horizontal transport of pollutants was blocked (Fig. 5a). The mean temperature profile indicates that there was a near-surface inversion in the box area and the mean height of PBL was lower than 500 m before 0900 BST on October 18 (Fig. 6), resulting in restricted atmospheric turbulence exchange in the vertical direction. As the variation in sea level pressure was small, the height of PBL was low and there was a near-surface inversion before 0900 BST in the polluted area, the effects of the horizontal and vertical transport on the pollutant concentrations reduction were limited in this episode. The decrease of pollutant concentrations between 0500 BST to 0900 BST on October 18 was mainly due to the deposition. The 2-h accumulated rainfall (Fig. 7) shows that the rain belts present a northeast-southwest orientation. During the period of 0500–0700 BST, the rainfall in the western Chengdu was 1.5–2 mm, and that in the western Meishan and northern Leshan was 1–1.5 mm. The rainfall increased from 0700 to 0900 BST, and the pollutants decreased most obviously during this period. At 0900 BST on October 18, the near-surface inversion was broken, both the height of PBL and the gradient of sea level pressure increased, resulting in a faster reduction of pollutants. Fig. 8 shows the difference of air pollutant concentrations before (0500 BST) and after the rainfall intensification (1300 BST). Concentrations of  $\text{PM}_{2.5}$ ,  $\text{PM}_{10}$ ,  $\text{SO}_2$  and  $\text{NO}_2$  in the southwestern Chengdu, western Meishan were all reduced by more than  $60 \mu\text{g m}^{-3}$  from 0500 BST to 1300 BST. This initially indicates that the rainfall has a significant effect of removing these four air pollutants. The  $\text{O}_3$  concentrations increased in most areas, reflecting that the influence mechanisms of  $\text{O}_3$  concentrations might be different from those of other air pollutants. Such rainfall episodes and

rainfall intensity cannot reflect its ability in removing  $\text{O}_3$ .

#### 4.2. Variations in the average concentrations of air pollutants in Chengdu

The observation results (Fig. 9) show that from 2000 BST on October 17, the concentrations of main air pollutants in Chengdu gradually decreased, especially for  $\text{PM}_{2.5}$ ,  $\text{PM}_{10}$  and  $\text{NO}_2$ . The  $\text{SO}_2$  concentrations slightly decreased, while the  $\text{O}_3$  concentrations fluctuated. The dotted and solid reference lines indicate the moment when the average rainfall increases by observation and simulation, respectively. Fig. 10a shows the average hourly rainfall at Wenjiang, Shuangliu, Xindu, Pixian, Longquanyi and Dujiangyan stations in Chengdu from 2000 BST on October 17 to 1800 BST on October 18. The stations close to the air quality monitoring station are selected, and the solid lines represents the simulation results. The observation results indicate that the average hourly rainfall in Chengdu was small, but the rainfall duration was rather long. The concentrations of air pollutants decreased rapidly at 2000 BST. At that time, the average wind speed in Chengdu was relatively small ( $1.2 \text{ m s}^{-1}$ ), and the average wind direction abruptly changed at 2100 BST (Fig. 10b). However, the decreasing trend of concentrations remained unaffected, which indicates that the wind speed and wind direction are not the main factors attributing to the variation in concentrations of pollutants. The simulation results show that the dominant wind direction in Chengdu was southeast and the average wind speed was about  $1.0\text{--}1.4 \text{ m s}^{-1}$  between 2000 BST on October 17 and 0400 BST on October 18. There was an  $\text{PM}_{2.5}$ ,  $\text{PM}_{10}$ ,  $\text{SO}_2$  and  $\text{NO}_2$  accumulated area in the southwest of Chengdu. Despite the low wind speed, the southerly wind might cause the pollutants to

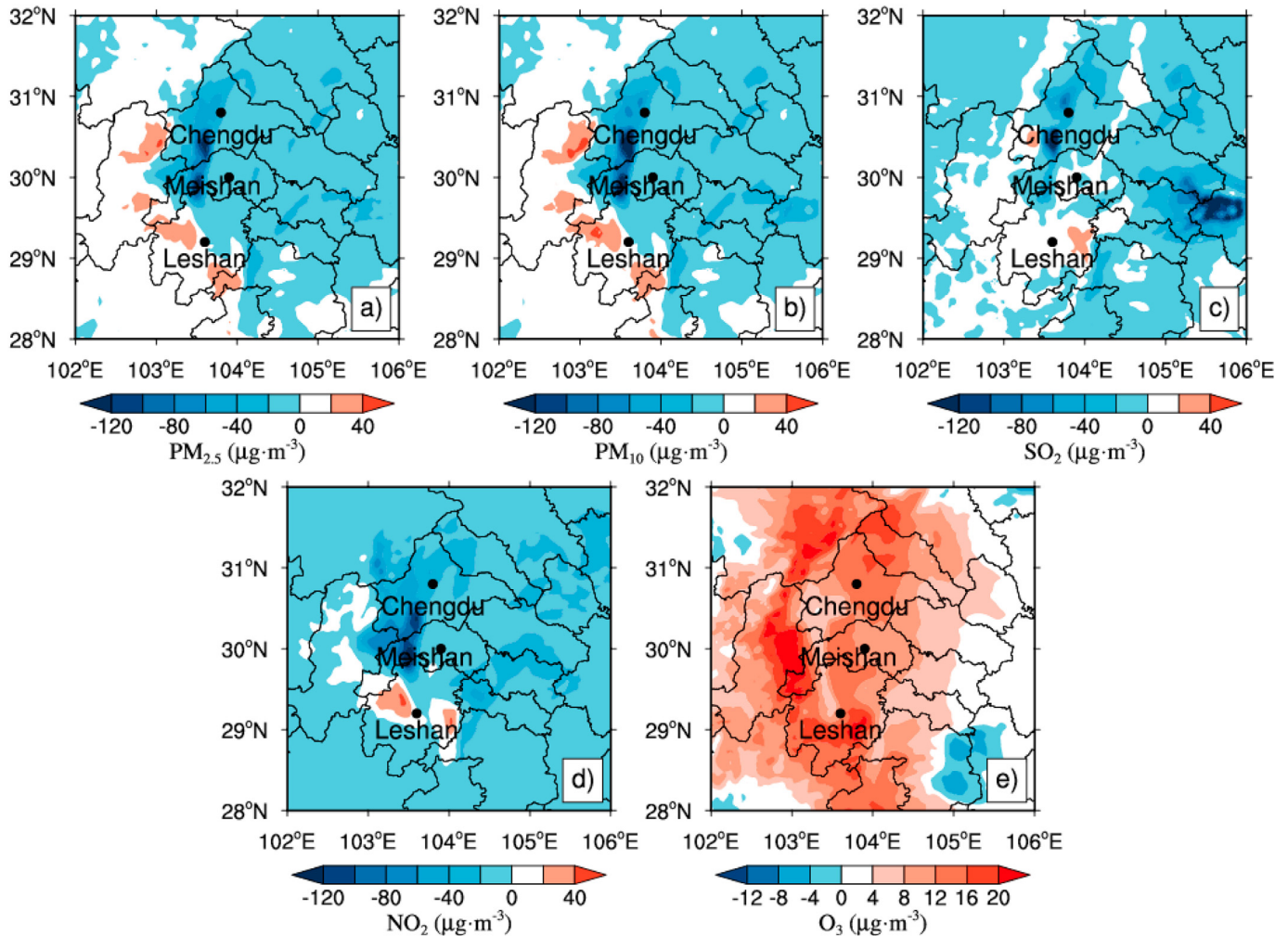


**Fig. 8.** The differences of  $\text{PM}_{2.5}$  (a),  $\text{PM}_{10}$  (b),  $\text{SO}_2$  (c),  $\text{NO}_2$  (d) and  $\text{O}_3$  (e) between 0500 and 1300 BST (Units:  $\mu\text{g}\cdot\text{m}^{-3}$ ).

spread from the pollution source area to the central Chengdu. The hourly rainfall by simulation from 1800 BST on October 17 to 0200 BST on October 18 in Chengdu was underestimated. The decreasing trend of the average concentrations of air pollutants between 2000 BST on October 17 and 0200 BST on October 18 in Chengdu was not reproduced in the simulation. Therefore, the simulation did not reproduce the decreasing trend of pollutants mainly because of the underestimation of rainfall and the component of southerly wind, indicating that the simulation of the model on the wind field and precipitation can greatly affect the simulation results of pollutant concentrations. Due to the rainfall episode (although the average hourly intensity was very small), the concentrations of  $\text{PM}_{2.5}$ ,  $\text{PM}_{10}$  and other air pollutants output by the model have decreased since 0400 BST on October 18 as the rainfall duration increased, although the height of PBL still decreased. Fig. 11a shows that during the period from 2200 BST on October 17 to 0000 BST on October 18, the pollutants near the ground increased, while the pollutants at the level of 300 m–2500 m decreased. The soluble salts are significantly reduced (Fig. 12a), and the particle size of the reduced aerosol is almost all above 0.15625  $\mu\text{m}$  (size bins are from 03 to 08, refer to Table 2). The cross-section of dBZ (Fig. 13) shows that the cloud was below the isotherm of 0 °C, which could be considered as warm cloud. Aerosols participating in the warm cloud process are generally hygroscopic large nuclei ( $> 0.1 \mu\text{m}$ ). When the pollutants involve soluble salts with strong hygroscopicity, they may be activated under low supersaturation. Generally, they can work when the relative humidity is less than 100%. Fig. 12c shows that the average relative humidity of the air from 2200 to 0000 BST is up to 100%. In addition, as CCN (Cloud

condensation nuclei) increases, the cloud droplet number concentration will increase significantly, and the cloud water is also higher. Fig. 12b shows that the cloud water increases significantly above 400 m. Therefore, the pollutants at the level of 300 m–2500 m decreased because they acted as CCN in warm cloud process. At 0900 BST on October 18, the near-surface inversion was broken and the height of PBL increased (Fig. 11b). The pollutants near the ground were transported to high altitude and participated in the nucleation process. When raindrops fall, pollutants are carried to the ground. Finally, the pollutants from the ground to the high altitude were decreased (Fig. 11c). By 1000 BST on October 18, the concentrations of pollutants near the ground has decreased by over 50  $\mu\text{g}\cdot\text{m}^{-3}$ .

From 2100 BST on October 17 to 0800 BST on October 18, the simulated rainfall intensity was smaller than the observation, whereas the  $\text{NO}_2$  concentrations still decreased, indicating that the removal of  $\text{NO}_2$  by rainfall was not related to the rainfall intensity. Besides, the wind speed was relatively small during this period, and the correlation coefficient between the wind speed and the  $\text{NO}_2$  concentrations in this period was less than 0.4, so the wind speed was not the main reason for the decrease of  $\text{NO}_2$  concentrations in this period either. For  $\text{O}_3$ , as a photochemical product, its concentrations has obvious diurnal variation, which is generally high in daytime and low from night to the next early morning. The WRF-Chem reproduced this diurnal cycle of  $\text{O}_3$ , but the fluctuation between 0000 and 0600 BST on October 18 was not simulated, and the reason might be that it was an occasional  $\text{O}_3$  emission event.

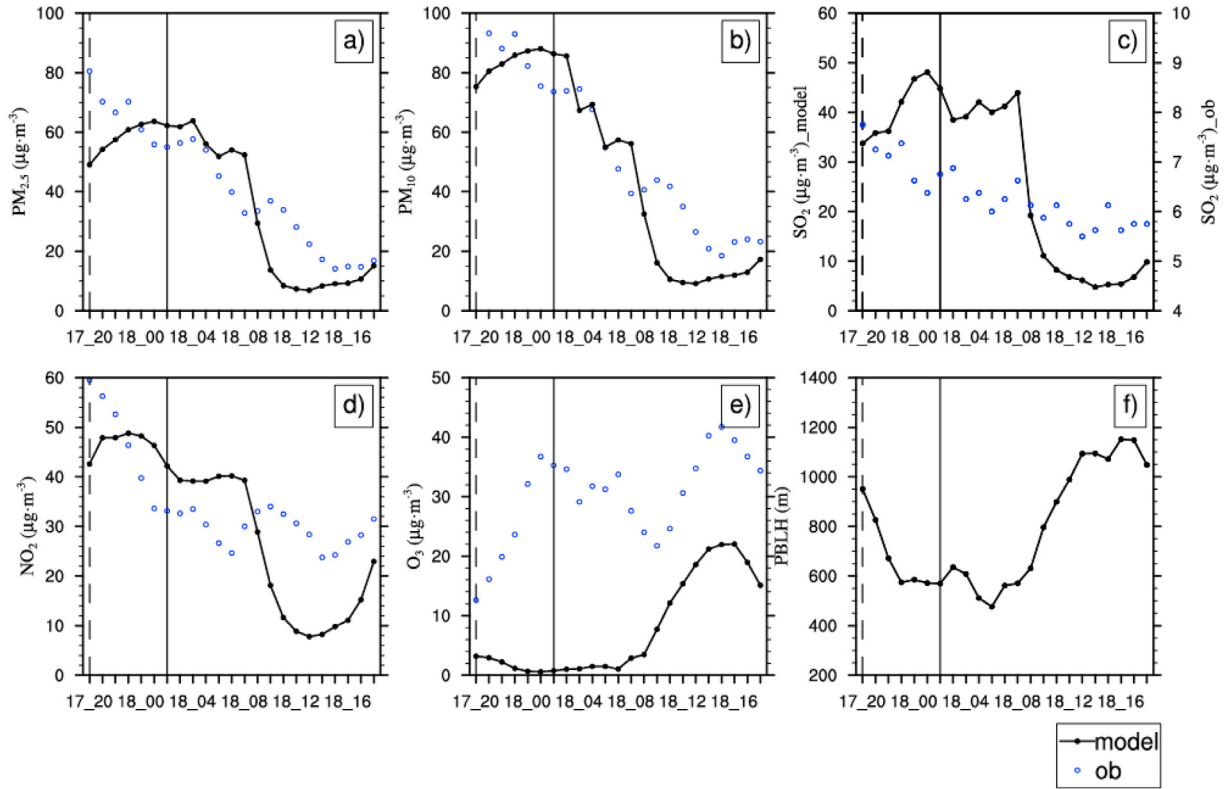


**Fig. 9.** Comparison between simulation results (solid lines) and hourly observations (scatter) of PM<sub>2.5</sub> (a), PM<sub>10</sub> (b), SO<sub>2</sub> (c), NO<sub>2</sub> (d) and O<sub>3</sub> (e) in Chengdu from 2000 BST on 17 October to 1800 BST on 18 October, 2018.

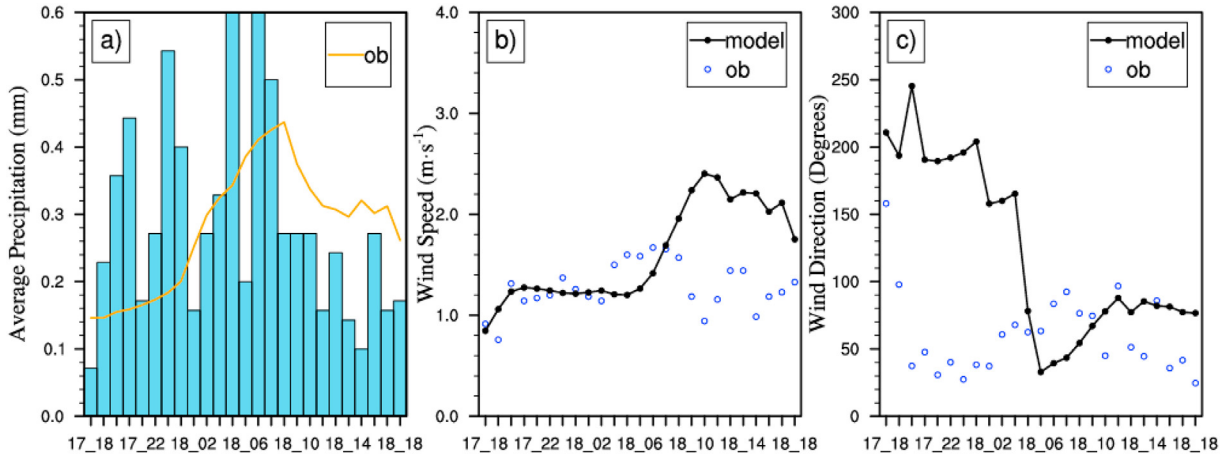
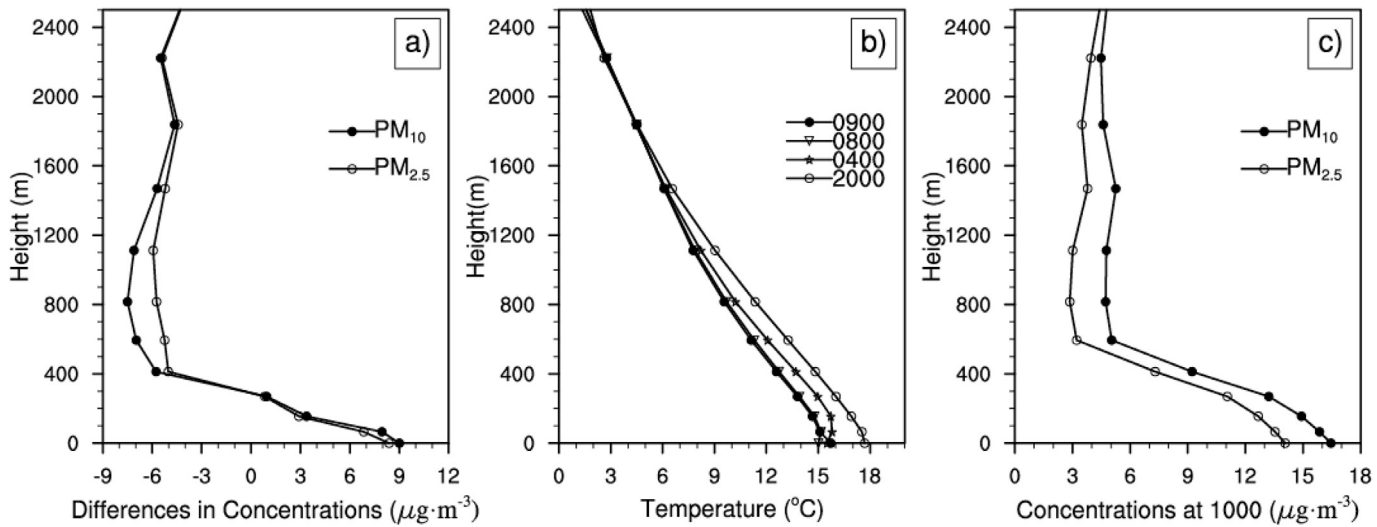


**Fig. 10.** Comparison between observed results and simulation results (solid lines) of hourly rainfall (a), average wind speed (b) and direction (c) in Chengdu from 18000 BST on 17 October to 1800 BST on 18 October, 2018.

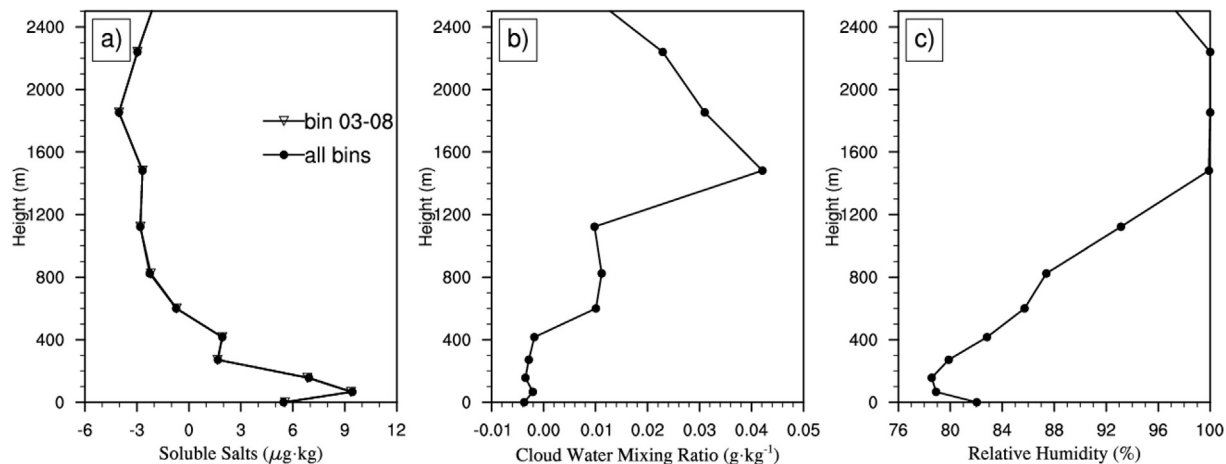
#### 4.3. Variations for air pollutant concentrations at stations

Fig. 14 shows the time series of air pollutant concentrations at Dashixilu station (DSXL) and LYS. DSXL (30.656°N, 104.024°E) represents the downtown area of Chengdu, while LYS (31.028°N, 103.613°E) represents the suburban areas. To analyze the wet removal effects of PM<sub>2.5</sub>, PM<sub>10</sub> and NO<sub>2</sub> by the rainfall, the air pollutant concentrations, wind direction, wind speed, PBL, temperature stratification curve, sea level pressure and hourly rainfall at these two stations are discussed. From 2000 BST on October 17 to 0400 BST on October 18, the concentrations of particulate pollutants in DSXL fluctuated slightly, and the PM<sub>10</sub> concentrations were slightly underestimated. During this period, the PBL remained above 700 m, and there was a near-surface inversion below 150 m. The wind direction changed twice obviously,

which was basically the same with that of the fluctuation. The fluctuation of the concentrations was mainly affected by wind speed and wind direction. From 0400 to 0600 BST, there was very little rainfall and the concentrations of particulate pollutants increased rapidly, with an approximate range of 25–30 µg m⁻³, and the NO<sub>2</sub> concentrations also increased by 15 µg m⁻³. There was no significant change in wind speed or wind direction compared with the situation before the concentrations increased, while the PBL lowered by 350 m during this period. Therefore, the increase in the concentrations of three air pollutants was mainly due to the lowering of the boundary layer, concentrating the pollutants in a small height range. When the rainfall lasted for several hours, the concentrations of pollutants began to decline since 0700 BST on October 18 (Fig. 14). The reference line indicates the time point when the rainfall increases. The wind speed and



**Fig. 11.** a) The profile of difference in particle matters between 2200 BST on 17 October and 0000 BST on October 18, b) The profile of temperature, c) The profile of particle matters at 1000 on October 18.



**Fig. 12.** a) The profile of difference in soluble salts (a) and cloud water (b) between 2200 BST on 17 October and 0000 BST on October 18, c) The profile of average relative humidity from 2200 BST to 0000 BST.

the height of PBL increased from 0900 BST and the wind direction gradually changed from northeasterly to easterly. The concentrations of  $\text{PM}_{2.5}$  and  $\text{PM}_{10}$  decreased more rapidly due to the increase of both the wind speed and PBLH. By 1200 BST on October 18, the concentrations of  $\text{PM}_{2.5}$ ,  $\text{PM}_{10}$  and  $\text{NO}_2$  were all as low as  $10 \mu\text{g m}^{-3}$ , with a decrease range of more than  $50 \mu\text{g m}^{-3}$ . The  $\text{NO}_2$  concentrations decreased continuously from 2100 BST on October 17 to 0400 BST on October 18. During this period, the wind speed and rainfall were relatively small, but the relative humidity was about 72%–88% and continuously increased, there was an anti-correlation between  $\text{NO}_2$  concentrations and the relative humidity with the fitting coefficient reaching  $-0.75$ . From 1200 to 1800 BST, the concentrations of  $\text{PM}_{2.5}$ ,  $\text{PM}_{10}$  and  $\text{NO}_2$  increased slightly by  $15$ – $20 \mu\text{g m}^{-3}$ . During this period, the height of PBL and wind speed still maintained at a high level, but the rainfall decreased significantly, indicating that the smaller intensity of rainfall could only slow down the increase of air pollutant concentrations. From 1800 BST on October 17 to 1800 BST on October 18, the variations in the concentrations of  $\text{PM}_{2.5}$ ,  $\text{PM}_{10}$ ,  $\text{NO}_2$  and  $\text{SO}_2$  were closely related to the rainfall, wind speed and PBL height. Among them,  $\text{PM}_{2.5}$ ,  $\text{PM}_{10}$  and  $\text{NO}_2$  were mostly affected by the rainfall and wind speed, with the correlation coefficient reaching  $-0.78$ . The  $\text{SO}_2$  concentrations was strongly anti-correlated with the height of PBL.

Since 2000 BST on October 17, the concentrations of air pollutants

in LYS decreased steadily. The initial concentrations of pollutants were relatively low and the variations in concentrations were relatively small at LYS station because there was less pollution emission. The concentrations of  $\text{PM}_{2.5}$  and  $\text{PM}_{10}$  decreased by  $15 \mu\text{g m}^{-3}$  from 2000 BST on October 17 to 0800 BST on October 18, while those of  $\text{SO}_2$  and  $\text{NO}_2$  decreased by  $30 \mu\text{g m}^{-3}$  and  $55 \mu\text{g m}^{-3}$ , respectively. The model overestimated the initial concentrations of  $\text{SO}_2$  and  $\text{NO}_2$ , but the variation trends in concentrations were reproduced well, and thus the deviation of the initial concentrations could be attributed to the emission inventory. Since 1800 BST on October 17, the rainfall at LYS has gradually increased, and the correlation coefficients of the  $\text{PM}_{2.5}$  and  $\text{PM}_{10}$  concentrations with the hourly rainfall were  $-0.59$  and  $-0.60$ , respectively (Table 5). Besides, the correlation coefficients of  $\text{SO}_2$  and  $\text{NO}_2$  concentrations with the hourly rainfall reached  $-0.96$  and  $-0.81$ , respectively. Therefore, when the initial concentrations were low, the concentrations of air pollutants were closely related to the rainfall intensity. After 1200 BST, the rainfall intensity decreased, while the concentrations of air pollutants rose slightly. According to the temperature stratification curve, there was no inversion or isothermal layer from the near surface to the upper air. The surface synoptic situation was the same as that when the concentrations decreased. The PBL remained at a high level, and the wind speed decreased slightly ( $1.8 \text{ m s}^{-1}$ ). The correlations of the pollutant concentrations with the

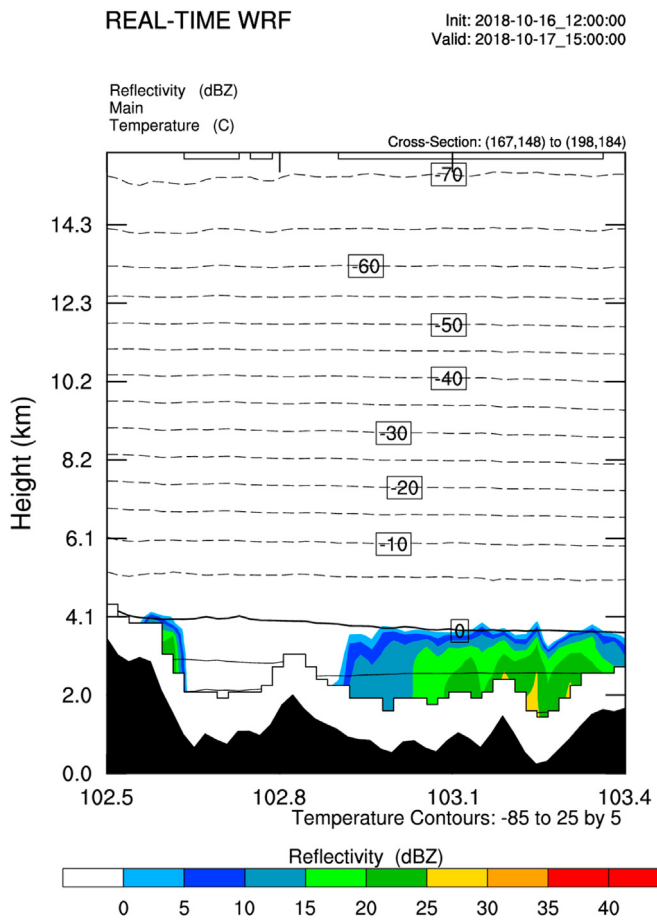


Fig. 13. The cross-section ( $102.5^{\circ}\text{E}$ ,  $29.5^{\circ}\text{N}$  ~  $103.5^{\circ}\text{E}$ ,  $30.5^{\circ}\text{N}$ ) of dBZ at 2300 BST on October 17, 2018.

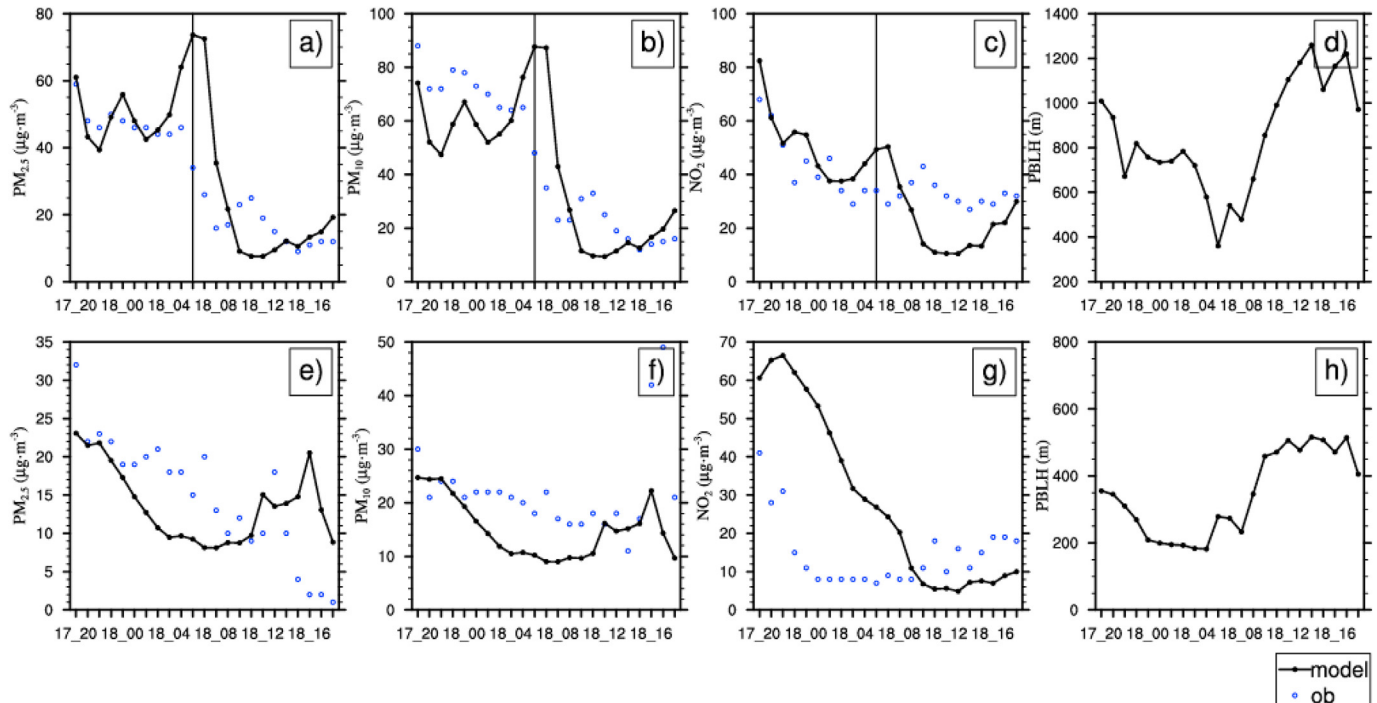


Fig. 14. Comparison between simulation results (solid lines) and hourly observations (scatter) of  $\text{PM}_{2.5}$ ,  $\text{PM}_{10}$  and  $\text{NO}_2$  at DSXL station (a, b, c) and LYS station (e, f, g) from 2000 on 17, October to 18:00 on October 18, 2018.

wind speed and the PBL height were poor, all of which were no more than  $-0.45$ . Therefore, this increase was mainly due to the limited removal effect of small-magnitude rainfall on aerosol concentrations after the concentrations decreased to a certain extent.

## 5. Conclusions

In this study, the WRF-Chem model is used to simulate a rainfall episode in Sichuan Basin. The model simulations are compared with the ground-based observation data to evaluate the feasibility of the model. The spatio-temporal distribution and evolution of air pollutants before and after the rainfall in the plain area, and the effects of rainfall and other major meteorological factors on the concentrations of  $\text{PM}_{2.5}$ ,  $\text{PM}_{10}$ ,  $\text{SO}_2$ ,  $\text{NO}_2$  and  $\text{O}_3$  are further analyzed. The results of evaluation show that the model overestimates T2 by  $1.68^{\circ}\text{C}$ , underestimates RH2 by  $-15.56\%$  on average, and overestimates WS10 by  $0.15 \text{ m s}^{-1}$ . The HR for wind speed is as high as  $93.1\%$ ; the bias of WD10 is  $12.61^{\circ}$ ; and the NMBs of four major meteorological elements are less than  $20\%$ . The simulation results on wind field and precipitation greatly affect the simulation of air pollutants. This model underestimates the concentrations of most air pollutants. The biases between the simulations and observations for  $\text{PM}_{2.5}$ ,  $\text{PM}_{10}$ ,  $\text{NO}_2$ ,  $\text{CO}$ ,  $\text{O}_3$  and  $\text{SO}_2$  concentrations are  $-34.62\%$ ,  $-39.35\%$ ,  $-10.78\%$ ,  $-4.37\%$ ,  $-75.59\%$  and  $300\%$ , respectively. The MFBs (MFEs) of  $\text{PM}_{2.5}$ ,  $\text{PM}_{10}$ ,  $\text{NO}_2$ , and  $\text{CO}$  concentrations range from  $-12.21\%$  to  $-31.22\%$  ( $28.13\%-39.59\%$ ), reaching a higher performance standard. The MFEs of  $\text{SO}_2$  are slightly higher than the  $75\%$  performance standard, and the MFEs of  $\text{O}_3$  are  $71.27\%$ , which is still within the standard range of MFE. The effects of meteorological factors on pollutants are as follows.

The small gradient of sea level pressure (less than  $1 \text{ hPa}$ ) and the near-surface inversion in the Chengdu Plain are conducive to the accumulation of air pollutants in the area, and vice versa. Continuous rainfall with small-magnitude rainfall ( $0.3\text{--}0.5 \text{ mm h}^{-1}$ ) has an obvious effect in reducing the concentrations of  $\text{PM}_{2.5}$ ,  $\text{PM}_{10}$ ,  $\text{SO}_2$  and  $\text{NO}_2$ , although both horizontal and vertical diffusion are unfavorable. The influence mechanism of  $\text{O}_3$  concentrations is different from those of

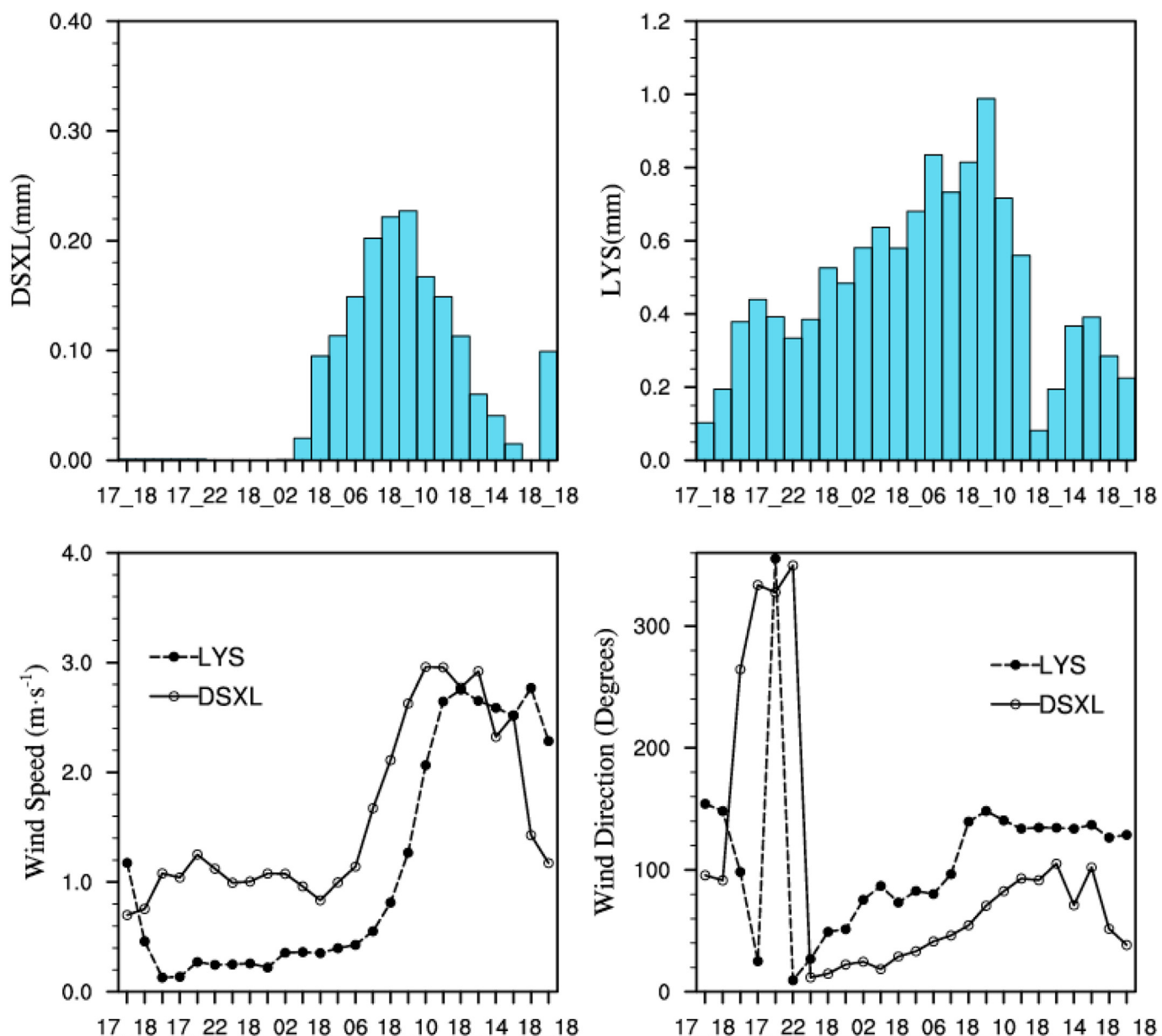


Fig. 15. Hourly rainfall, wind speed and wind direction at DSXL station and LYS station from 1800 on 17 October to 1800 on 18 October, 2018.

Table 5

Correlation coefficient between air pollutants concentrations and major meteorological factors.

	DSXL station				LYS station			
	PM <sub>2.5</sub>	PM <sub>10</sub>	SO <sub>2</sub>	NO <sub>2</sub>	PM <sub>2.5</sub>	PM <sub>10</sub>	SO <sub>2</sub>	NO <sub>2</sub>
Hourly rainfall	-0.5437	-0.5428	-0.4652	-0.4893	-0.5761	-0.5981	-0.9571	-0.8097
Total rainfall	-0.7821	-0.7778	-0.7638	0.8339	-0.3051	-0.3310	-0.8936	-0.6566
Wind speed	-0.8451	-0.8558	-0.7735	-0.8188	-0.1646	-0.1132	-0.8082	-0.4531
PBLH	-0.7323	-0.7304	-0.8122	-0.4838	0.1325	0.1048	-0.6551	-0.2827

other air pollutants, the rainfall of  $0.3\text{--}0.5 \text{ mm h}^{-1}$  has almost no wet removal effect on O<sub>3</sub>. There is an upper limit of the impact of continuous rainfall on air pollutants. Moreover, when the concentrations of pollutants drop to a certain level, the wet deposition by rainfall will decrease. The concentrations of particulate pollutants decrease as a result of participation in the nucleation process. When rainfall occurs and vertical diffusion is not restricted, the concentrations of pollutants on the ground are reduced more quickly by being transported to high

altitude. Under the influence of nucleation scavenging and impaction scavenging, the pollutants from the ground to the high altitude will decrease. In urban areas with near-surface inversion, the concentrations of air pollutants decrease when the wind speed is high and increase when the wind speed decreases. The correlation coefficients for the concentrations of PM<sub>2.5</sub>, PM<sub>10</sub>, SO<sub>2</sub> and NO<sub>2</sub> with the wind speed are -0.85, -0.86, -0.77 and -0.82, respectively. In suburban stations with the small initial concentrations, the concentrations have strong

correlations with the rainfall intensity, but have little to do with the PBL and the wind speed.

The model configurations used in this study reproduced both meteorological field and pollutants well, which can provide a reference for the parameterization schemes of numerical simulation in Sichuan Basin. In addition, the effects of rainfall and other meteorological fields on air pollutants during rainfall episode discussed in this study, which can provide guidance for prediction and manual intervention of air pollution.

#### Credit author statement

**Wei Long:** conceived, Methodology, analyzed the data, Writing - original draft. **Yunjun Zhou:** conceived, Methodology, analyzed the data, Writing - original draft. **Ping Liu:** supplied the analytical data.

#### Declaration of competing interest

We declare that we have no known competing financial interests or personal relationships that could have appeared to influence the work reported in this paper.

#### Acknowledgements

This work was supported by the National Natural Science Foundation of China (41875169), the National Key R&D Program of China(2018YFC1505702), the Guizhou Provincial Science and Technology Program (2019-2387), the Chengdu Science and Technology Anti-haze Project(2018-ZM01-00038-SN), and the Education Department of Sichuan Province(16CZ0021).

#### References

- Boylan, J.W., Russell, A.G., 2006. PM and light extinction model performance metrics, goals, and criteria for three-dimensional air quality models. *Atmos. Environ.* 40 (26), 4946–4959.
- Chate, D.M., 2005. Study of scavenging of submicron-sized aerosol particles by thunderstorm rain events. *Atmos. Environ.* 39 (35), 6608–6619.
- Chen, F., Dudhia, Jimy. Coupling an advanced land surface-hydrology model with the penn state-NCAR MM5 modeling system. Part I: model implementation and sensitivity. *Mon. Weather Rev.* 129(4):569-585.
- Dong, Q., Zhao, P., Chen, Y., 2016. Impact of collision removal of rainfall on aerosol particles of different sizes. *Environ. Sci.* 37 (10), 3686–3692.
- Geng, T., Tong, H., Zhao, X., Zhu, Y., 2019. Effect of wet deposition on the removal efficiency of particulate matter in the yangtze-huaihe region. *O. Res. Environ. Sci.* 32 (2), 273–283.
- Greenfield, S.M., 1956. Rain scavenging of radioactive particulate matter from the atmosphere. *J. Atmos. Sci.* 14 (14), 115–125.
- Grell, G.A., Peckham, S.E., Schmitz, R., et al., 2005. Fully coupled “online” chemistry within the WRF model. *Atmos. Environ.* 39 (37), 6957–6975.
- He, X., Ma, J., Xu, J., et al., 2016. Simulation of a heavy PM2.5 pollutant event over beijing-tianjin-hebei region in october 2014[J]. *Meteorol. Mon.* 42 (7), 827–837.
- Holt, T., Raman, S., 1988. A review and comparative evaluation of multilevel boundary layer parameterizations for first-order and turbulent kinetic energy closure schemes. *Rev. Geophys.* 26 (4), 761.
- Hu, X.M., Nielsen-Gammon, J.W., Zhang, F., 2010. Evaluation of three planetary boundary layer schemes in the WRF model. *J. Appl. Meteorol. Clim.* 49 (9), 1831–1844.
- Iacono, M.J., Delamere, J.S., Mlawer, E.J., et al., 2008. Radiative forcing by long-lived greenhouse gases: calculations with the AER radiative transfer models. *J. Geophys. Res. Atmos.* 113 (D13).
- Jiang, W., Xie, W., Wang, B., et al., 2019. Analysis on the characteristics of heavy pollution atmospheric circulation in the Sichuan Basin from 2014 to 2016. *Acta Sci. Circumstantiae* 39, 180–188 (01).
- Kang, H., Zhu, B., Fan, S., 2009. Size distributions and wet scavenging properties of winter aerosol particles in North Suburb of Nanjing. *Clim. Environ. Res.* 14, 523–530 (05).
- Li, R., Wang, X., 2007. Effects of precipitation on air pollution in urumqi city. *O. Desert Oasis Meteorol* 2, 13–15.
- Li, M., Zhang, Q., Streets, D.G., He, K.B., Cheng, Y.F., Emmons, L.K., Huo, H., Kang, S.C., Lu, Z., Shao, M., Su, H., Yu, X., Zhang, Y., 2014. Mapping Asian anthropogenic emissions of non-methane volatile organic compounds to multiple chemical mechanisms. *Atmos. Chem. Phys.* 14, 5617–5638. <https://doi.org/10.5194/acp-14-5617-2014>.
- Liao, T., Wang, S., Ai, J., et al., 2017. Heavy pollution episodes, transport pathways and potential sources of PM2.5 during the winter of 2013 in Chengdu (China). *Sci. Total Environ.* 584/585, 1056–1065.
- Lin, Y.L., Farley, R.D., Orville, H.D., 1983. Bulk parameterization of the snow field in a cloud model. *J. Clim. Appl. Meteorol.* 22 (6), 1065–1092.
- Liu, F., Zhang, Q., Tong, D., Zheng, B., Li, M., Huo, H., He, K.B., 2015. High-resolution inventory of technologies, activities, and emissions of coal-fired power plants in China from 1990 to 2010. *Atmos. Chem. Phys.* 15, 13299–13317. <https://doi.org/10.5194/acp-15-13299-2015>.
- Long, Q., Chen, J., Liao, T., et al., 2019. The severe pollution process, transport pathways and potential sources of particulate matter during the winter of 2016 in leshan city. *Res. Environ. Sci.* 32, 263–272 (02).
- Misenis, C., Zhang, Y., 2010. An examination of sensitivity of WRF/Chem predictions to physical parameterizations, horizontal grid spacing, and nesting options. *Atmos. Res.* 97 (3) 0-334.
- Nakanishi, M., Niino, H., 2006. An improved mellor-yamada level-3 model: its numerical stability and application to a regional prediction of advection fog. *Bound. - Layer Meteorol.* 119 (2), 397–407.
- Ouyang, Z., Liao, T., Chen, K., et al., 2019. Comparative analysis of winter air stagnation characteristics and air quality improvement assessment in Sichuan Basin and Beijing-Tianjin-Hebei Region from 2014 to 2017. *Acta Sci. Circumstantiae* 39, 2353–2361 (07).
- Pang, Y., Han, Z., Zhu, B., Li, J., 2013. A model study on distribution and evolution of atmospheric pollutants over Beijing-Tianjin-Hebei region in summertime with WRF-Chem. *Trans. Atmos. Sci.* 36, 674–682 (06).
- Tie, X., Geng, F., Peng, L., et al., 2009. Measurement and modeling of O3 variability in Shanghai, China: application of the WRF-Chem model. *Atmos. Environ.* 43 (28), 4289–4302.
- Tie, X., Zhang, Q., He, H., et al., 2015. A budget analysis of the formation of haze in Beijing. *Atmos. Environ.* 100, 25–36.
- Tuccella, P., Curci, G., Visconti, G., et al., 2012. Modeling of gas and aerosol with WRF-Chem over Europe: evaluation and sensitivity study. *J. Geophys. Res. Atmos.* 117 (D3).
- Wang, L., Zhang, Y., Wang, K., 2016. Application of weather research and forecasting model with chemistry (WRF/chem) over northern China: sensitivity study, comparative evaluation, and policy implications. *Atmos. Environ.* 124 (JAN.PT.B), 337–350.
- Wild, O., Zhu, X., Prather, M.J., 2000. Fast-J: accurate simulation of in- and below-cloud photolysis in tropospheric chemical models. *J. Atmos. Chem.* 37 (3), 245–282.
- Yang, L., Wang, S., Zhang, Y., 2018. Variation characteristics of air pollutant concentrations and their effects on precipitation in Chengdu area in the recent three years. *J. Lanzhou Univ.* 54, 731–738 (06).
- Yu, C., Deng, X., Shi, C., et al., 2018. The scavenging effect of precipitation and wind on PM2.5 and PM10. *Acta Sci. Circumstantiae* 38 (12), 4620–4629.
- Zaveri, R.A., Easter, R.C., Fast, J.D., et al., 2008. Model for simulating aerosol interactions and chemistry (MOSAIC). *J. Geophys. Res. Atmos.* 113 (D13).
- Zaveri, R.A., Peters, L.K., 1999. A new lumped structure photochemical mechanism for large-scale applications. *J. Geophys. Res.* 104 (D23), 30387.
- Zeng, S., Wang, Y., 2016. Researches of weather pattern and pollution meteorological characteristics in Chengdu area. *Resour. Environ. Yangtze Basin* 25 (S1), 59–67.
- Zeng, S., Zhang, Y., 2017. The effect of meteorological elements on continuing heavy air pollution: a case study in the Chengdu area during the 2014 spring festival. *Atmos* 8 (12).
- Zhang, B., Liu, S., Ma, Y., 2012. The effect of MYJ and YSU schemes on the simulation of boundary layer meteorological factors of WRF. *Chin. J. Geophys.* 5, 2239–2248 (07).
- Zhang, L., Wang, T., Lv, M., et al., 2015. On the severe haze in Beijing during January 2013: unravelling the effects of meteorological anomalies with. *WRF-Chem. Atmos. Environ.* 104, 11–21.
- Zhang, Q., Streets, D.G., Carmichael, G.R., He, K.B., Huo, H., Kannari, A., Klimont, Z., Park, I.S., Reddy, S., Fu, J.S., Chen, D., Duan, L., Lei, Y., Wang, L.T., Yao, Z.L., 2009. Asian emissions in 2006 for the NASA INTEX-B mission. *Atmos. Chem. Phys.* 9, 5131–5153.
- Zhao, P., Tuygun, G.T., Li, B., et al., 2019. The effect of environmental regulations on air quality: a long-term trend analysis of SO<sub>2</sub> and NO<sub>2</sub> in the largest urban agglomeration in southwest China. *Atmos. Pollut. Res.* 10, 2030–2039.
- Zhao, S., Yu, Y., He, J., et al., 2015. Below-cloud scavenging of aerosol particles by precipitation in a typical valley city, northwestern China. *Atmos. Environ.* 102, 70–78.
- Zheng, B., Huo, H., Zhang, Q., Yao, Z.L., Wang, X.T., Yang, X.F., Liu, H., He, K.B., 2014. High-resolution mapping of vehicle emissions in China in 2008. *Atmos. Chem. Phys.* 14, 9787–9805. <https://doi.org/10.5194/acp-14-9787-2014>.
- Zhou, B., Liu, D., Wei, J., et al., 2015. A preliminary analysis in scavenging effect of precipitation on aerosol particles. *Resour. Environ. Yangtze Basin* (S1), 160–170.
- Zhou, G., Wang, S., Chen, X., 2013. Study on the removal efficiency of precipitation to air pollutants in the main urban area of Chongqing. *Environ. Pollut. Control.* 35, 112 (09).
- Zou, C., Huang, H., Yang, F., et al., 2017. Atmospheric particulate and gaseous pollutants removal efficiency by rainfall and the influencing factors. *Environ. Sci. Technol.* 40, 133–140 (01).